SUPPORTING INFORMATION

Multifunctional Carbon Nanotubes Covalently Coated by Imine-based Covalent Organic Frameworks: Exploring Structure-Property Relationships through Nanomechanics

Alicia Moya,[a] Mercedes Hernando-Pérez,[b] Marta Pérez-Illana,[b] Carmen San Martín,[b] Julio Gómez-Herrero,[a,c] José Alemán,*[d,e] Rubén Mas-Ballesté,*[e,f] Pedro J. de Pablo*[a,c]

[a]Department of Condense Matter Physics (module 03). Universidad Autónoma de Madrid, 28049 Madrid (Spain). E-mail: p.j.depablo@uam.es

[b]Department of Structure of Macromolecules. Centro Nacional de Biotecnología-CSIC, 28049 Madrid (Spain).

[c]Institute of Condense Matter Physics (IFIMAC). Universidad Autónoma de Madrid, 28049 Madrid (Spain).

[d]Department of Organic Chemistry (module 01). Universidad Autónoma de Madrid, 28049 Madrid (Spain). E-mail: jose.aleman.lara@gmail.com

[e]Institute for Advanced Research in Chemical Sciences (IAdChem). Universidad Autónoma de Madrid, 28049 Madrid (Spain). E-mail: ruben.mas@uam.es

[f]Department of Inorganic Chemistry (module 07). Universidad Autónoma de Madrid, 28049 Madrid (Spain).

Calibration of the AFM and cantilever spring constant

A simple method to calibrate the frictional force from lateral force and topographical images using an atomic force microscope has been performed using a rectangular silicon nitride AFM cantilevers with the following dimensions: 800 nm thick, 100 µm long and 20 µm wide. Its normal spring constant and frequency resonance is routinely calibrated using Seder's method[44] before all the experiments and obtaining values of 68-74 kHz and 0.29-0.35 N/m, respectively. From the formula described in experimental section,

we obtain the lateral spring constant of the cantilever, K_L = 690-832 N/m, which will be used for the calibration of the frictional force.

When the tip is laterally moving, the focused laser on the cantilever changes its angle of reflection on the photodetector. These changes are registered by a voltage signal, which must be calibrated into force units. For such propose, the lateral calibration factor was determined using Si-grating with step heights of 20.3 ± 1.5 nm height. Lateral force images were acquired for such a grid and converted into force curves to calculate the lateral calibration factor. The increase of the lateral force when the AFM tip touches the step of the grid is recorded as an abrupt change of the lateral force and, from the slope, we obtain a calibration factor in units of V/nm. The calibrated value obtained from different lateral forces images results 0.022 V/nm. Finally, the voltage signal of the lateral force is converted to Newtons using the lateral spring constant and the above calibrated value.

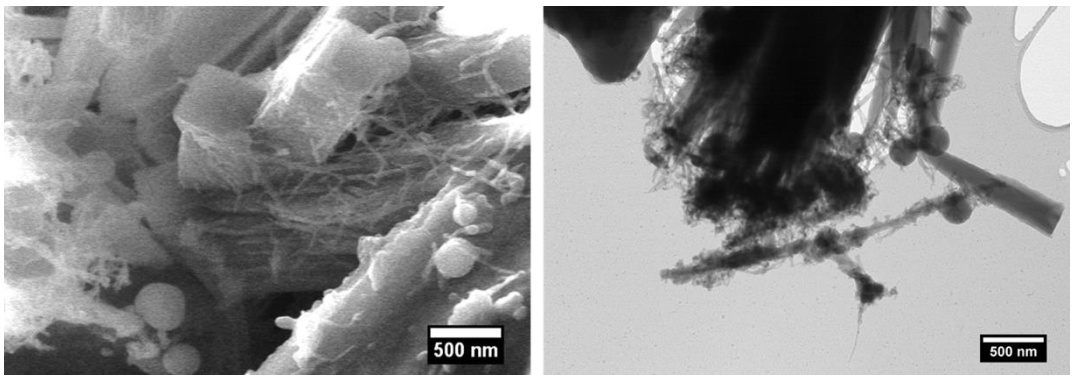

Figure S1. SEM and TEM image of the control sample referred as p-MWCNTs@COF.

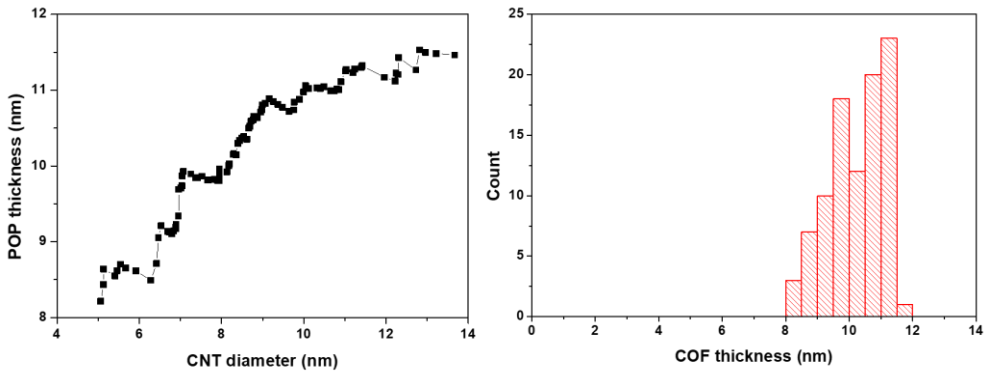

Figure S2. Left: Relation between the COF thickness and the CNT diameter. Right: Distribution of the COF thickness measured from TEM images.

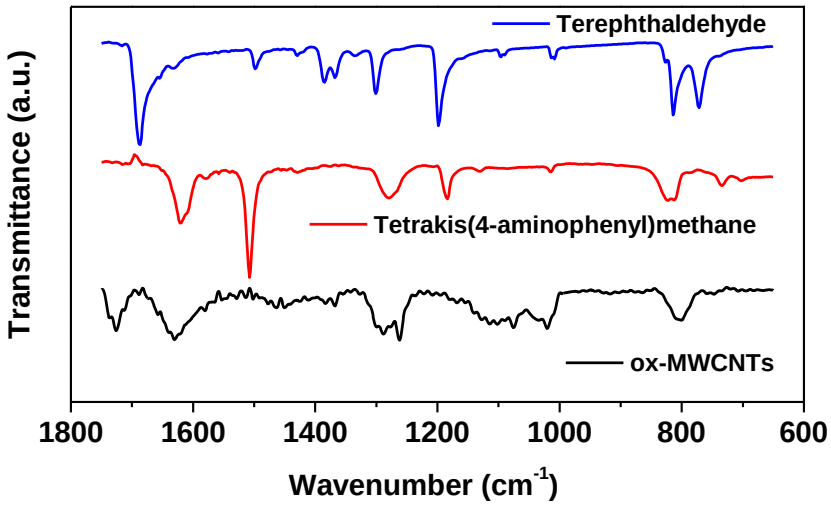

Figure S3. FT-IR spectra of ox-MWCNTs (black curve) and COF precursors: tetrakis(4-aminophenyl)methane (red curve) and terephthaldehyde (green curve).

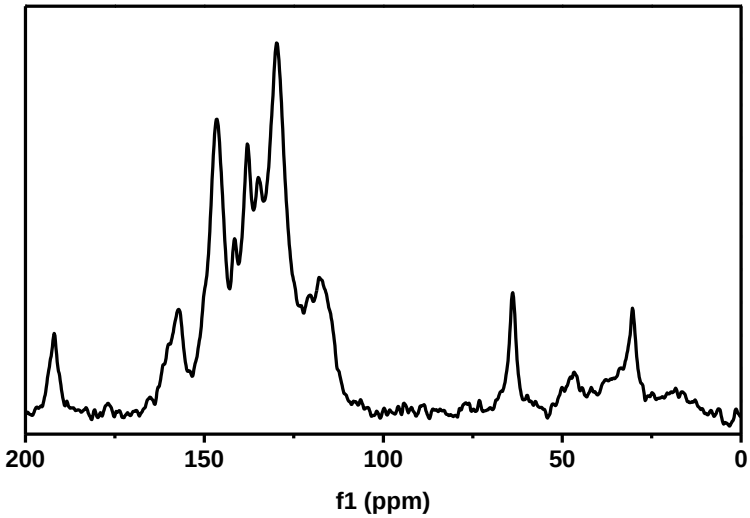

Figure S4. Solid-state ^{13}C CP-MAS spectrum of synthesized ox-MWCNTs@COF hybrid material. The characteristic chemical ^{13}C-NMR shifts in ppm hybrid are assigned in the table below.

Table S1. Signal assignment of ^{13}C-NMR spectra of Figure S4.

Signal	Assignment
30.33	Solvent
63.84	Aliphatic quaternary: α-aromatic
117.89	Aromatic: β-aliphatic, γ-imine
129.77	Aromatic: β-vinyl

134.9	Aromatic: α-aliphatic, p-imine
137.94	Aromatic: α-vinyl
141.53	Aromatic: α-carbonyl
146.54	Aromatic: β-imine, γ-aliphatic
157.23	Alkene: α-imine, α-aromatic
191.97	Carbonyl: α-aromatic

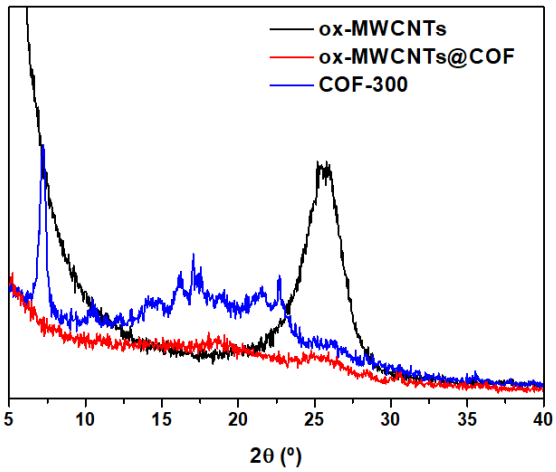

Figure S5. X-ray diffraction pattern of ox-MWCNTs, COF-300 and ox-MWCNTs@COF hybrid material.

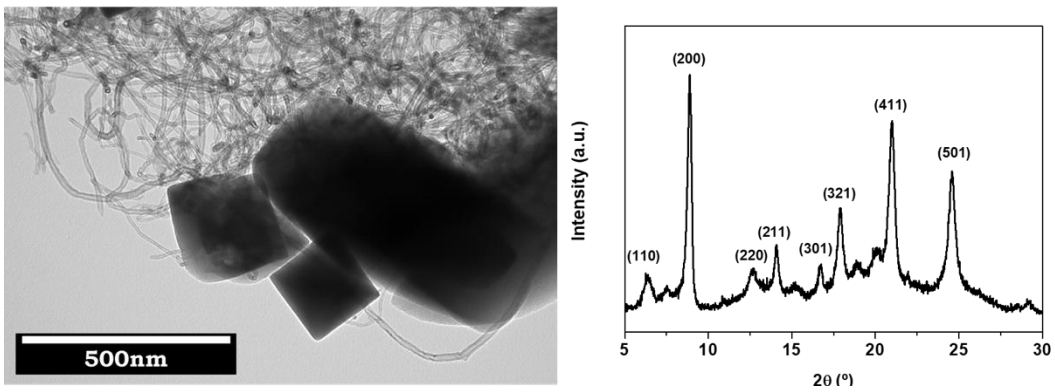

Figure S6. TEM image of the crystallized ox-MWCNTs@COF material (left) its corresponding XRD pattern (right).

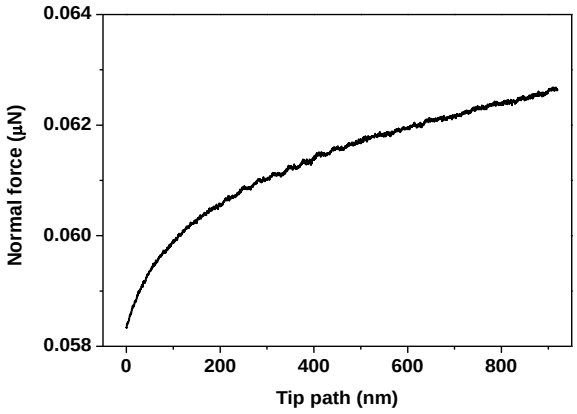

Figure S7. Normal force as a function of the AFM tip path corresponding to the fracture of the individual ox-MWCNTs@COF hybrid nanotube showed in Figure 4.

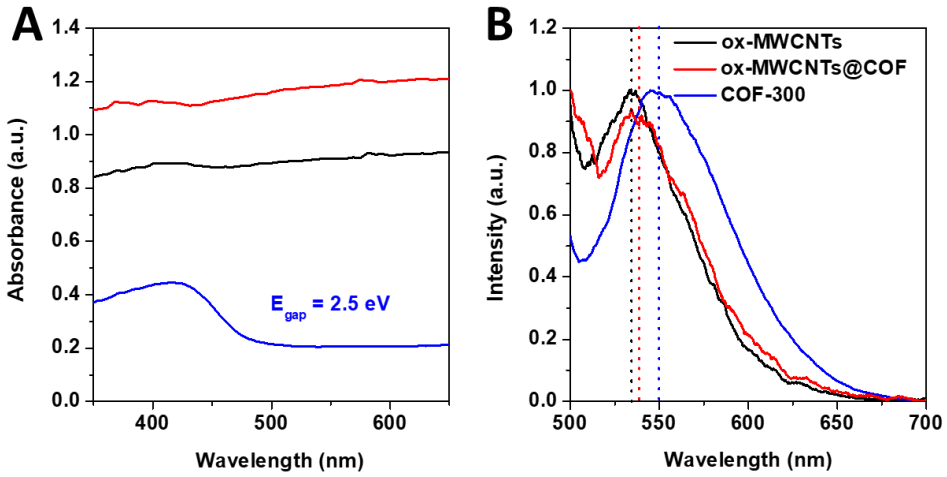

Figure S8. Optical properties of ox-MWCNTs (black curve), ox-MWCNTs@COF (red curve) and COF-300 (blue curve): a) absorption spectra and b) emission spectra.

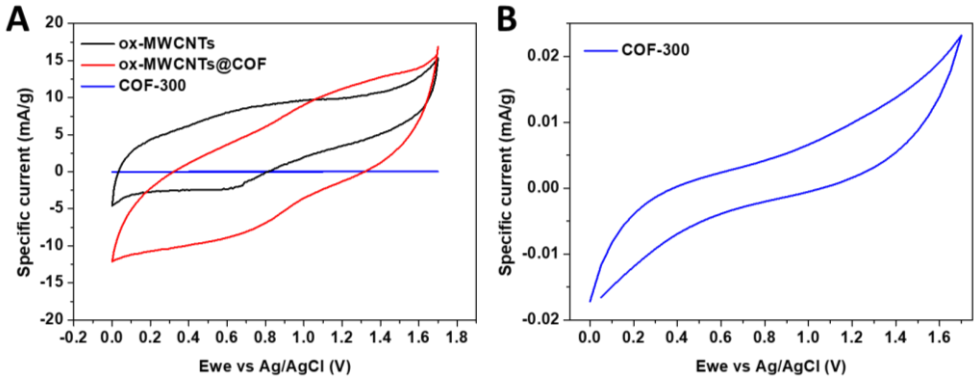

Figure S9. Electrochemical cyclic voltammetries of the of ox-MWCNTs (black curve), ox-MWCNTs@COF (red curve) and COF-300 (blue curve) materials tested at a scan rate of 50 mV/s.

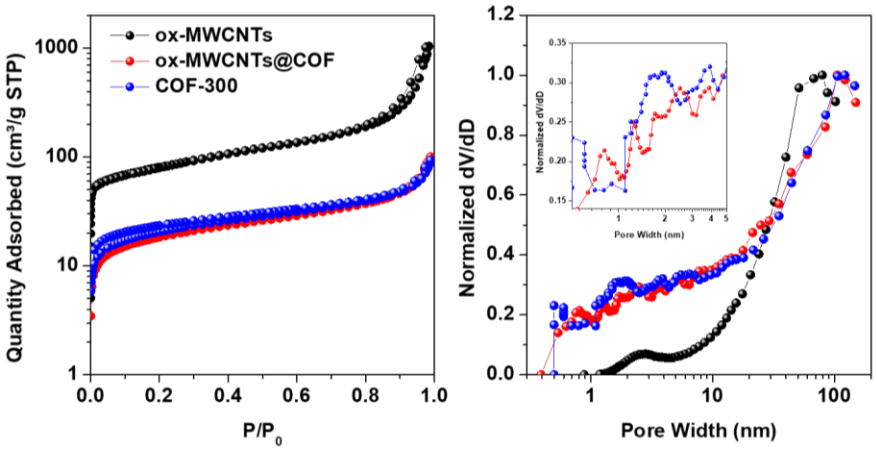

Figure S10. N_2 adsorption isotherms (left) and pore size distribution (right) of ox-MWCNTs, COF-300 and ox-MWCNTs@COF hybrid material.

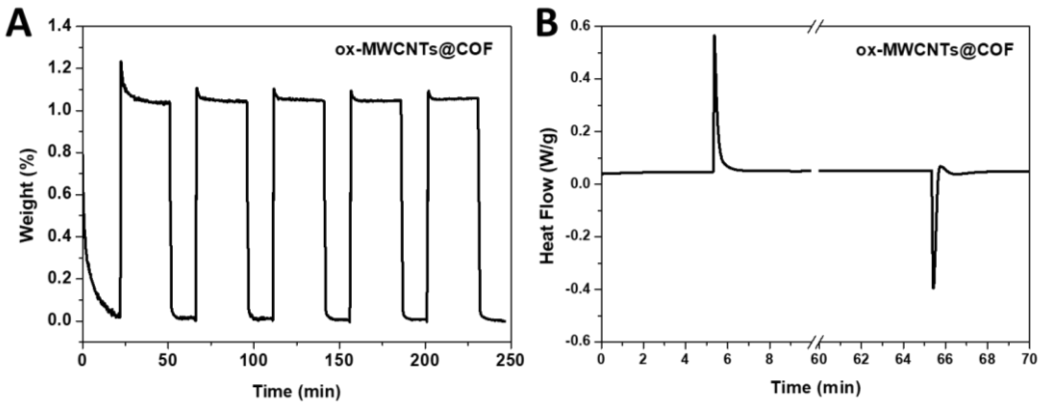

Figure S11. a) Cycling test and b) DSC curve of the CO_2 adsorption and desorption on the ox-MWCNTs@COF hybrid material at 25°C.

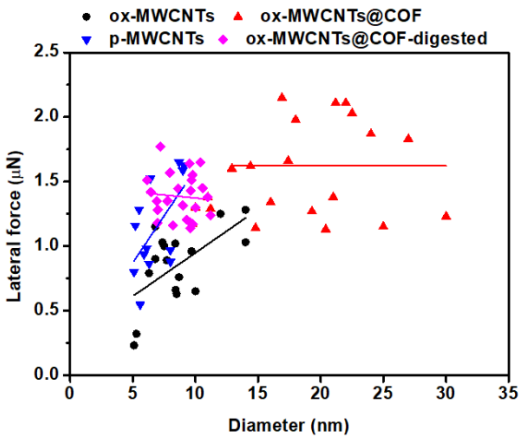

Figure S12. Effect of the diameter in the lateral force for cutting nanotubes of ox-MWCNTs, ox-MWCNTs@COF, p-MWCNTs and ox-MWCNTs@COF-digested.

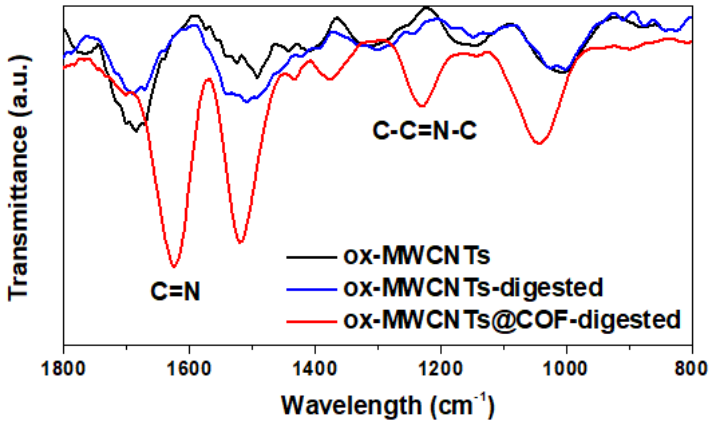

Figure S13. FT-IR spectra of ox-MWCNTs (black curve) and ox-MWCNTs and hybrid treated with aniline (blue and red curve, respectively).

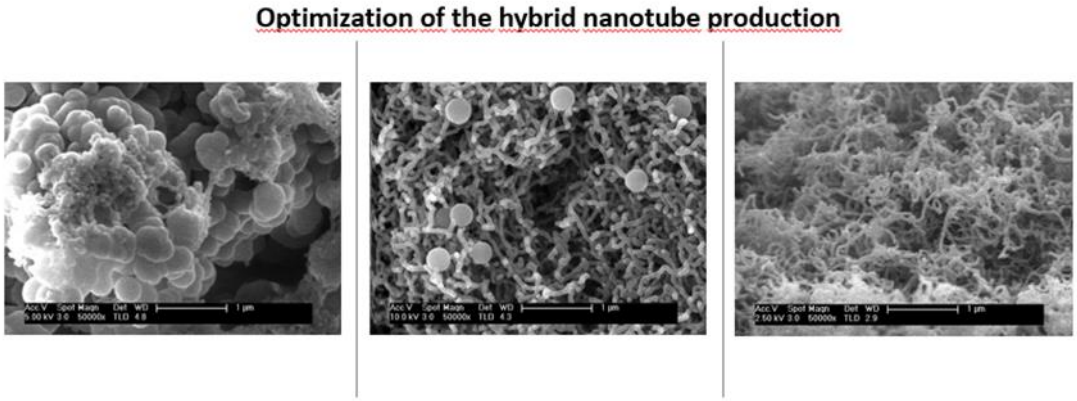

Figure S14. SEM images SEM images showing the optimization of the synthesis. Left image shows mainly COF spheres and some coated nanotubes; middle image shows a mixture of COF spheres and hybrid nanotubes and right image shows a homogeneous hybrid material.